Journal of Porous Materials 9: 243–256, 2002

Surface Charge of Variable Porosity Al_2O_3(s) and SiO_2(s) Adsorbents

KEITH W. GOYNE
Department of Crop and Soil Sciences, The Pennsylvania State University, University Park, PA 16802, USA; Department of Soil, Water and Environmental Science, University of Arizona, Tucson, AZ 85721, USA

ANDREW R. ZIMMERMAN
Department of Geosciences, The Pennsylvania State University, PA 16802, USA

BHARAT L. NEWALKAR AND SRIDHAR KOMARNENI
Materials Research Laboratory, The Pennsylvania State University, University Park, PA 16802, USA

SUSAN L. BRANTLEY
Department of Geosciences, The Pennsylvania State University, PA 16802, USA

JON CHOROVER
Department of Soil, Water and Environmental Science, University of Arizona, Tucson, AZ 85721, USA
chorover@ag.arizona.edu

Received June 29, 2002; Revised September 20, 2002

Abstract. The surface charge properties of two SiO_2 and three Al_2O_3 mineral adsorbents with varying degrees of framework porosity were investigated using discontinuous titration and ion adsorption methodologies. Points of zero net charge (p.z.n.c) for porous and non-porous SiO_2 were <2.82 and for Al_2O_3 minerals ranged from 6.47–6.87. Silica surfaces possessed very slight negative charge in the acid pH range (pH < 7) and significant dissociation of silanol groups occurred at pH > 7. Variation of surface charge density with aqueous proton concentration was nearly identical within a mineral type (i.e., SiO_2 or Al_2O_3) irrespective of the degree of framework porosity, indicating that the densities of dissociable surface sites are equivalent, when normalized to surface area. The results suggest that the use of titration methods alone may be insufficient for thorough surface charge characterization, particularly at low and high pH. Proton titrations should be coupled with concurrent ion adsorption measurements to confirm surface charge development. Discontinuous proton titration and ion adsorption data, which were in agreement in the slightly acidic through slightly basic pH range, both indicated that p.z.n.c. was equal to the point of zero net proton charge (p.z.n.p.c.) for the variable charge minerals investigated.

Keywords: surface charge, proton adsorption, ion adsorption, site density, alumina, silica, p.z.n.p.c.

1. Introduction

Porous materials with varying metal composition ratios are being evaluated and used as molecular sieves [1, 2], catalysts [3, 4], humidity sensors [5] and contaminant barriers [6]. In particular, recent studies (e.g., [6]) propose the use of microporous (pores <2 nm) and mesoporous (2–50 nm) minerals as adsorbents for pollutants

in aqueous systems. However, to utilize these materials for maximum economic and environmental benefits, relationships between physical properties (e.g., specific surface area and pore structure) and surface chemistry (e.g., surface charge, adsorption behavior) must be elucidated. Despite the importance of charge properties to sorption of ionic and neutral solutes, pH-dependent surface charge of synthetic mesoporous minerals has not been investigated in detail. Without this information it is difficult to assess whether compound sorption differences between porous and non-porous materials are due to porosity itself or to co-varying differences in reactive site density. For instance, Goyne et al. [7] observed significantly greater adsorption of 2,4-dichlorophenoxyacetic acid to mesoporous alumina, relative to non-porous alumina, in surface normalized batch adsorption experiments. However, it is unclear if these differences were attributable to mesoporosity or increased reactive site density present on the porous alumina surface. In addition, a thorough understanding of points of zero charge, active site density and reactivity, as affected by porosity will enable researchers to select porous materials for specific applications to aqueous systems (e.g., ion or contaminant adsorption).

Surface charge on natural and synthesized minerals can develop in three principal ways: (a) as a result of proton or other ion complexation at the particle surface, (b) from lattice imperfections at the particle surface, and (c) isomorphous substitution within the crystal structure [8]. With regard to synthetic silica and alumina minerals, surface complexation reactions are expected to be the dominant source of surface charge.

Net total particle surface-charge, σ_P, is defined quantitatively as the sum of four components [9]:

$$\sigma_P = \sigma_O + \sigma_H + \sigma_{IS} + \sigma_{OS} \quad (1)$$

where σ_O is the net permanent structural-charge density due to isomorphic substitutions; σ_H is the net proton surface-charge density created by the difference between the moles of protons and hydroxide ions complexed by surface functional groups; σ_{IS} is the net inner-sphere complex surface-charge density resulting from net total charge of ions (excluding H^+ and OH^-) bound into inner-sphere surface coordination; and σ_{OS} is the net outer-sphere complex surface-charge density resulting from net total charge of ions (excluding H^+ and OH^-) bound into outer-sphere surface coordination. If σ_P is non-zero (i.e., the particle possesses charge), then the law of surface charge balance requires that σ_P be balanced by the diffuse layer surface-charge density, σ_D, which is equal in magnitude, but opposite in sign to σ_P [9]:

$$\sigma_P = -\sigma_D \quad (2)$$

Ions in the diffuse layer are subjected to counteracting diffusion and electrostatic gradients such that they move freely in solution but a net diffuse ion swarm charge is sustained in local proximity to the surface, effectively balancing σ_P [10].

Points of zero charge are traditionally defined as pH values where one or more components of surface charge vanishes at a specified temperature, pressure, and aqueous solution composition [11]. The point of zero net charge (p.z.n.c.) is defined as the pH value where net adsorbed ion charge density (Δq) is equal to zero:

$$\Delta q = (q_+ - q_-) = \sigma_{IS} + \sigma_{OS} + \sigma_D \quad (3)$$

where q_+ and q_- refer to the adsorbed cation and anion charge, respectively, in units of moles of charge per square meter ($mol_c\ m^{-2}$).

The intrinsic surface-charge density, σ_{in}, represents components of surface charge developed from the mineral structure [11], which must be balanced by the adsorption of ions from solution:

$$\sigma_{in} = \sigma_O + \sigma_H = -\Delta q \quad (4)$$

The point of zero net proton charge (p.z.n.p.c.) is defined as the pH value where σ_H is equal to zero. Therefore, by Eq. (4), this is the pH value where σ_O is equal to $-\Delta q$. For variable charge minerals where σ_O is negligible or non-existent, p.z.n.c. must equal the p.z.n.p.c. (i.e., at the p.z.n.c., $\sigma_H = -\Delta q = 0$).

The introduction of mesoporosity into colloidal particles significantly alters the specific surface area of the solid phase. However, the extent to which chemical reactivity (e.g., surface acidity, ion affinity) is affected is not known. In the present work, silica and alumina mineral adsorbents were synthesized with varying degrees of mesoporosity and their surface charge properties were measured in aqueous suspension. The objective was to assess the extent to which the introduction of framework mesoporosity affects particle surface charge, background ion adsorption, and dissolution behavior.

2. Experimental

2.1. Adsorbent Synthesis and Treatment

Five mineral adsorbents were used in the present work: (1) porous Al_2O_3 (Al-P_{242}), (2) less porous Al_2O_3 (Al-P_{141}), (3) non-porous Al_2O_3 (Al-NP_{37}), (4) porous SiO_2 (Si-P_{700}), and (5) non-porous SiO_2 (Si-NP_8), where the subscripts refer to specific surface area in $m^2\ g^{-1}$. Al-NP_{37} and Si-NP_8 were purchased from Alfa Aesar (Ward Hill, MA) stock #'s 40007 and 89709, respectively. Al-NP_{37} was washed with 0.02 mol kg^{-1} $CaCl_2$ (0.208 kg L^{-1} suspension concentration) for 24 h in 250 ml polypropylene co-polymer centrifuge tubes at 7 rpm on an end-over-end mixer to remove an N-containing soluble constituent associated with synthesis. Suspensions were then centrifuged for 40 min at 18,830 g, followed by aspiration of the supernatant solution. This procedure was repeated, prior to washing the mineral twice with 95% ethanol to displace any entrained $CaCl_2$ solution. Following centrifugation and aspiration of the second ethanol wash, the mineral was oven-dried at 50°C for 48 h.

Al-P_{141} was prepared from boehmite supplied by CONDEA Vista Co. (Houston, TX) and is sold under the trade name Disperal. This mineral was calcined at 450°C for 24 h to induce dehydroxylation, thus creating a less-porous amorphous Al_2O_3.

Both Al-P_{242} and Si-P_{700} were prepared using a neutral template route [5, 12, 13]. The general procedure is as follows: 50.0 g of dodecylamine was mixed with 418.1 g ethanol and 532.8 g deionized water, followed by the addition of 204.2 g of aluminum isopropoxide or 208.3 g of tetraethyl orthosilicate under vigorous stirring. The mixture was then stirred for 30 min and aged at room temperature for 24 h. After aging, the sample was transferred to a glass plate and air-dried. The neutral template was removed from the air-dried materials by heating the minerals at 540°C for 6 h. Removal of the neutral template results in wormhole-like mesopores [13]. All minerals, except Si-NP_8, were ground gently prior to characterization. Samples were stored in polyethylene bottles prior to use.

2.2. Particle Characterization

Mean particle size of the powdered minerals used was determined by direct measurement of at least twenty particle diameters on TEM images (Philips EM420ST). Specific surface area (SSA) and pore structure of the adsorbents were examined using N_2 sorptometry (ASAP 2010, Micromeritics). Samples (0.5–2 g) were out-gassed for at least 6 h (150°C, 5 μm Hg) prior to analysis, and adsorption-desorption isotherms were measured at 77.4 K. SSA was estimated using multi-point adsorption data from the linear segment of the N_2 adsorption isotherms [14] in the relative pressure range 0.05 to 0.2 using Brunauer-Emmett-Teller (BET) theory. Pore size distributions were calculated from adsorption branch isotherms using the Barrett-Joyner-Halenda (BJH) method [15] assuming right cylindrical pores closed on one end and using the Halsey layer thickness equation [16].

Samples were analyzed for structural composition by diffuse reflectance infrared Fourier transform (DRIFT) spectroscopy. Adsorbents were weighed and mixed with ground KBr powder (Spectra-Tech, Inc.) to give a powdered sample concentration of 0.5 g kg^{-1}. All DRIFT spectra were obtained by averaging 400 scans at 2 cm^{-1} resolution on a Nicolet Magna 560 spectrometer. Powder X-ray diffraction (XRD) measurements were made on all samples, except Al-NP_{37}, using a Philips' X'pert diffractometer with Ni-filtered Cu K_α radiation. Al-NP_{37} was determined previously by Alfa Aesar (Ward Hill, MA) to be crystalline γ-Al_2O_3.

2.3. Variable Surface Charge

Surface charge density was measured for each adsorbent as a function of pH at fixed ionic strength (0.06 M) in a $CaCl_2$ background solution. A discontinuous titration procedure, which permits simultaneous measurement of proton and background electrolyte adsorption, including accounting for proton consumption in mineral dissolution reactions, was employed [17]. Minerals were suspended in a background electrolyte solution of $CaCl_2$/HCl or $CaCl_2$/$Ca(OH)_2$ ($I = 0.06$ M) to give a sorbent surface area in suspension of 2.29×10^3 m^2 L^{-1} in 50 ml Teflon or polypropylene co-polymer centrifuge tubes. This total surface area (measured by N_2 BET) is accessible to the adsorptive ions used in this study (H^+, OH^-, Ca^{2+}, Cl^-). Mixtures of the background electrolyte, acid and base were prepared to reach equilibrium supernatant solutions with $-\log [H^+]$ values ranging from 2 to 12. Blanks (no adsorbent) were prepared with the same mixtures of background electrolyte, acid and base used for the adsorbent suspensions. All suspensions and blanks were prepared in duplicate.

Suspensions and blanks were reacted on an end-over-end shaker (7 RPM) at 25°C in a temperature-controlled room for 24 h. Suspensions were then centrifuged at 15,290 g and 25° ± 2°C for 40 min, and supernatant solutions were aspirated into individual acid-washed 60 ml high density polyethylene (HDPE) bottles. An aliquot of solution was removed for measurement of electromotive force (emf), calibrated to proton *concentration* using an Orion-Ross model 8115 glass semi-micro combination electrode in conjunction with a Beckman Φ 390 pH meter reading in mV. Calibration of the electrode was performed using a Gran titration conducted at the same ionic strength as the supernatant solutions [17]. Experimental proton concentrations are reported as $-\log [H^+]$ in figures, but will be referred to as "pH" (for simplicity) hereafter in the text. The remaining sample was syringe-filtered through a 0.2 μm (nominal pore size) Gelman GHP Acrodisc and acidified to pH 2 by addition of trace metal grade HNO_3. Solutions were refrigerated (4°C) prior to chemical analysis. Blank solutions were treated in a similar manner, but they were not centrifuged or filtered.

Centrifuge tubes containing wet pellet adsorbents were weighed to determine the mass of entrained solution. Samples were then reacted with 0.020 kg of unbuffered 0.1 M NH_4NO_3 solution on an end-over-end shaker (7 RPM) for 8 h to displace adsorbed Ca^{2+} and Cl^-. Samples were removed and centrifuged at 15,290 g for 40 min. Supernatant solutions were aspirated into individual acid-washed, pre-weighed 60 ml HDPE bottles and filtered. This extraction step was repeated twice, solutions were combined quantitatively after filtration and the total solution mass was then measured and recorded. The NH_4NO_3 extracts were acidified to pH 2 by addition of trace metal grade HNO_3 and refrigerated prior to chemical analysis.

The concentrations of "index ions", Ca^{2+} and Cl^-, were determined by atomic absorption (AA) spectrophotometry (IL Video 22, Allied Analytical Systems) and ion chromatography (IC; DX500, Dionex Corp.), respectively, in both $CaCl_2$ and NH_4NO_3 solutions. Calibration standards were prepared on a mass basis in ultrapure (MilliQ UV-plus) water for $CaCl_2$ solutions and in 0.1 M NH_4NO_3 for NH_4NO_3 extracts. Dissolution of adsorbents during batch titration was assessed by measuring supernatant Al and Si concentrations using AA spectrophotometry or inductively-coupled plasma atomic emission spectroscopy (ICP-AES; Model 61E, Thermo Jarrell Ash). Calibration standards for Al and Si were prepared on a mass basis in $CaCl_2$ and NH_4NO_3 background electrolyte solutions using ICP reference standards (EM Science).

2.4. *Data Analysis*

The surface excess (q) of ion i, in $mol_c\ kg^{-1}$ of dry adsorbent, following a 24 h equilibrium period was calculated from:

$$q_i = |z_i| n_{i,(NH_4NO_3)} - M_{ent}|z_i| m_i \tag{5}$$

where z_i is the valence of ion i, $n_{i,(NH_4NO_3)}$ is the number of moles of ion i per unit dry adsorbent mass extracted in the NH_4NO_3 step, M_{ent} is the mass of entrained $CaCl_2$ solution per unit dry adsorbent mass, and m_i is the molinity (mol kg^{-1} of solution) of species i in the supernatant solution [10]. Surface excess values are reported for Ca^{2+} (q_+) and Cl^- (q_-). Readsorption of Al and Si following their dissolution was found to be negligible.

The net proton surface charge density, σ_H, was calculated for each pH from the difference between the final $[H^+]$ and $[OH^-]$ of a sample and corresponding blank (to account for adsorption or desorption of protons and hydroxide) corrected for proton or hydroxide consumption resulting from sorbent dissolution:

$$\sigma_H = M_{soln}\left\{([H^+]_b - [H^+]_s) - \left(\frac{K_{wc}}{[H^+]_b} - \frac{K_{wc}}{[H^+]_s}\right) + \left(-z_{avg}\sum [c_i]_{H^+,dissoln} + z_{avg}\sum [c_i]_{OH^-,dissoln}\right)\right\} \tag{6}$$

where M_{soln} is the mass of background electrolyte solution per unit dry adsorbent mass, $[H^+]$ is the concentration of protons in solution (mol kg^{-1}), K_{wc} is the conditional dissociation product of water at the experimental (0.06 M) ionic strength (1.57×10^{-14}; [18]). The subscripts s and b denote sample and blank, respectively. The correction for the consumption of H^+ or OH^- from solution because of Al or Si dissolution was made by multiplying the average valence, z_{avg}, which varies with pH (degree of hydrolysis), by the total aqueous concentration for a given element. The correction is negative for proton promoted dissolution (i.e., pH < point of minimum dissolution) and positive for hydroxide promoted dissolution (i.e., pH > point

of minimum dissolution) as indicated by the terms $-z_{avg}\sum[c_i]_{H^+,dissoln}$ and $z_{avg}\sum[c_i]_{OH^-,dissoln}$, respectively. In the absence of such a correction, the consumption of H^+ or OH^- would be erroneously attributed to charge development during adsorption. Aqueous speciation was calculated using ECOSAT [19]. All measured constituents were input to the model. Hydrolysis constants for Al and Si were obtained from Nordstrom and May [20] and Stumm and Morgan [21], respectively. Corrections for possible non-zero values of Eq. (6) at the p.z.n.p.c. [16] were found to increase disparities between σ_H and $-\Delta q$ and, therefore, were not included in this analysis.

The p.z.n.c. and p.z.n.p.c. values for each adsorbent were determined by non-linear, least-squares fitting of net ion adsorption data ($\Delta q, \sigma_H$) versus $-\log[H^+]$. The resulting equations were solved for $-\log[H^+]$, subject to the condition $\Delta q = 0$, to obtain the p.z.n.c. Assuming that these variable charge adsorbents contain no permanent structural charge then p.z.n.c. = p.z.n.p.c. This assumption was verified by comparing σ_H and Δq variation with pH.

3. Results and Discussion

3.1. Particle Characterization

The mean particle diameter of the five samples as determined by TEM are: 141 nm (Al-P_{242}), 105 nm (Al-P_{141}), 36 nm (Al-NP_{37}), 118 nm (Si-P_{700}), and 87 nm (Si-NP_8). Table 1 summarizes the SSA and pore characteristics of the five materials examined. While the SSA of Si-P_{700} differs greatly from that of Si-NP_8, the surface areas of the Al_2O_3 minerals fall within a narrower range (37–242 $m^2\ g^{-1}$). Variation in SSA for each sample can be attributed to their different pore structures (i.e., size and quantity).

We use the term "framework porosity" to refer to confined or intra-particle pores, whereas "textural porosity" refers to unconfined or inter-particle pores [12]. Mesoporosity is indicated in N_2 (g) adsorption isotherms both by the presence of adsorption-desorption hysteresis and by the slope of the adsorption step [12]. That is, a steeper N_2-adsorption step in the mid-relative pressure range of ca. 0.1 to 0.8 is indicative of relatively more framework mesoporosity [12]. Nitrogen adsorption isotherms for Si-P_{700} and Si-NP_8 (Fig. 1(a) and (b)) illustrate the characteristic isotherms (Types IV and II; [22]) of mesoporous framework and textural porosity, respectively. The isotherm shapes of Al-P_{242} and Al-P_{141} (Fig. 1(c) and (d)) are quite similar and display a character intemediate between (Types IV and II). However, framework porosity is indicated, by the discernable hysteresis expressed in both isotherms. The flatness of the Al-NP_{37} isotherm in the mid-pressure region (Fig. 1(e); Type II) indicates a lack of framework mesoporosity. None of these samples display isotherms typical of microporous samples (Type I; [22]).

Pore size distribution relative to pore volume for the five phases are shown in Fig. 2. In general, the pore sizes of the mesoporous materials are slightly greater and surface areas slightly less than those reported by Komarneni et al. [5] for silica and alumina minerals prepared by the same technique. Si-P_{700} exhibits the most monodisperse pore size distribution, with a mean pore diameter very similar to that of pore diameter of peak pore volume (3.2 nm, Fig. 2(a)), and also the greatest pore volume amongst the samples. In contrast, the

Table 1. Nitrogen adsorptometry-derived structural information of adsorbents.

Mineral		SSA[a] ($m^2\ g^{-1}$)	Pore Diam[b] (nm)	V_t[c] ($cm^3\ g^{-1}$)	SA_{fm}[d] (%)
Si-P_{700}	($n = 3$)	700 (±10)	3.43 (±0.02)	0.91 (±0.01)	99.7
Si-NP_8	($n = 3$)	7.5 (±0.1)	14 (±2)	0.024 (±0.003)	–[e]
Al-P_{242}	($n = 8$)	242 (±6)	8.2 (±0.6)	0.6 (±0.2)	96.5
Al-P_{141}	($n = 7$)	141 (±8)	9.6 (±0.6)	0.42 (±0.03)	92.6
Al-NP_{37}	($n = 6$)	37 (±3)	20 (±3)	0.20 (±0.01)	–[e]

[a]Mean specific surface area (±std. dev.) calculated by Brunauer-Emmett-Teller (BET) method.
[b]Mean pore diameter (±std. dev.) determined by the BJH method on the adsorption isotherm leg.
[c]Total pore volume determined by BJH method.
[d]Framework surface area (within pores 2–20 nm diameter) as percent of total determined by BJH method.
[e]Lack of adsorption/desorption hysteresis indicates absence of mesoporosity.

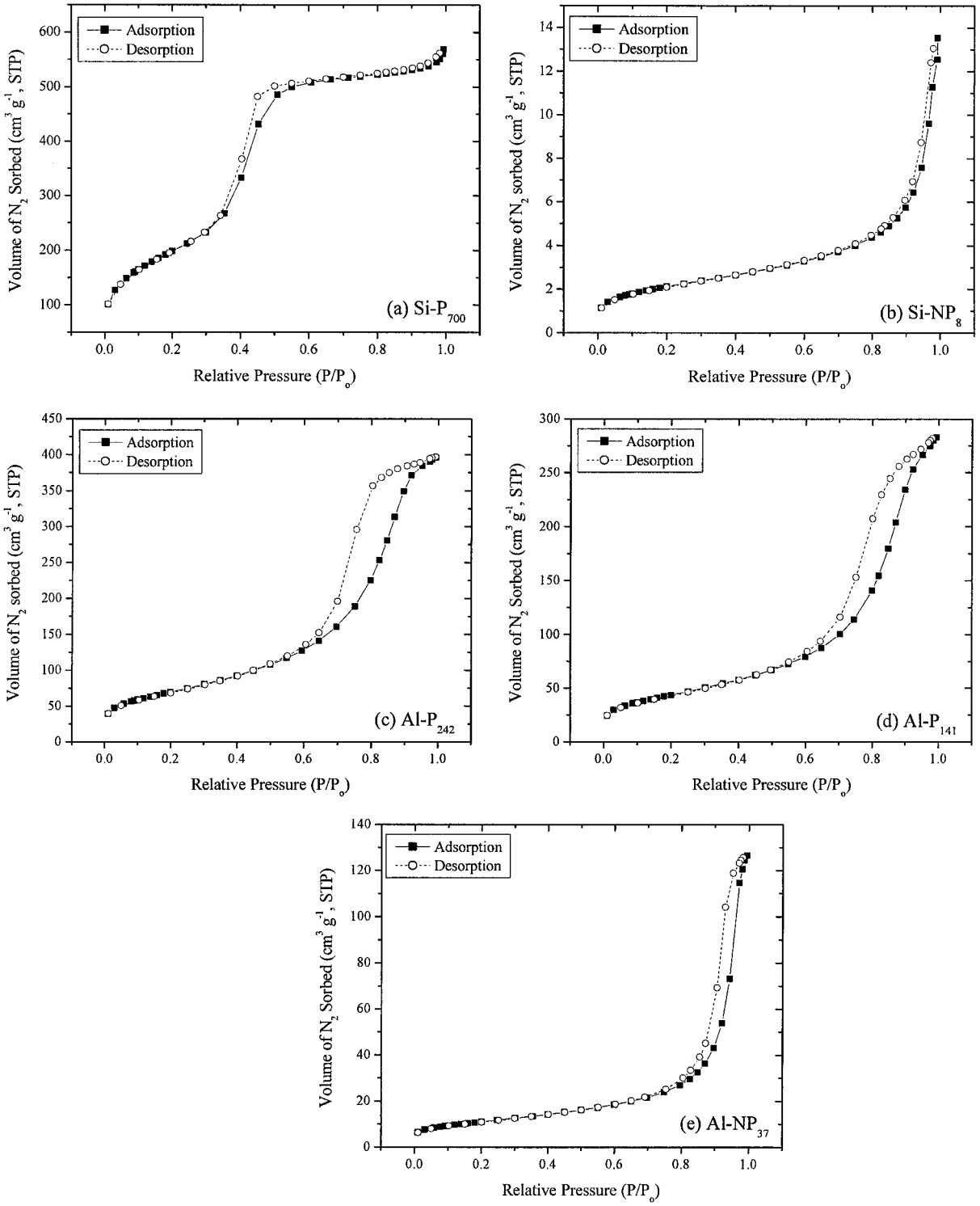

Figure 1. Nitrogen adsorption/desorption isotherms of adsorbents: (a) Si-P_{700}, (b) Si-NP_8, (c) Al-P_{242}, (d) Al-P_{141}, (e) Al-NP_{37}. Note different *y*-axis scales.

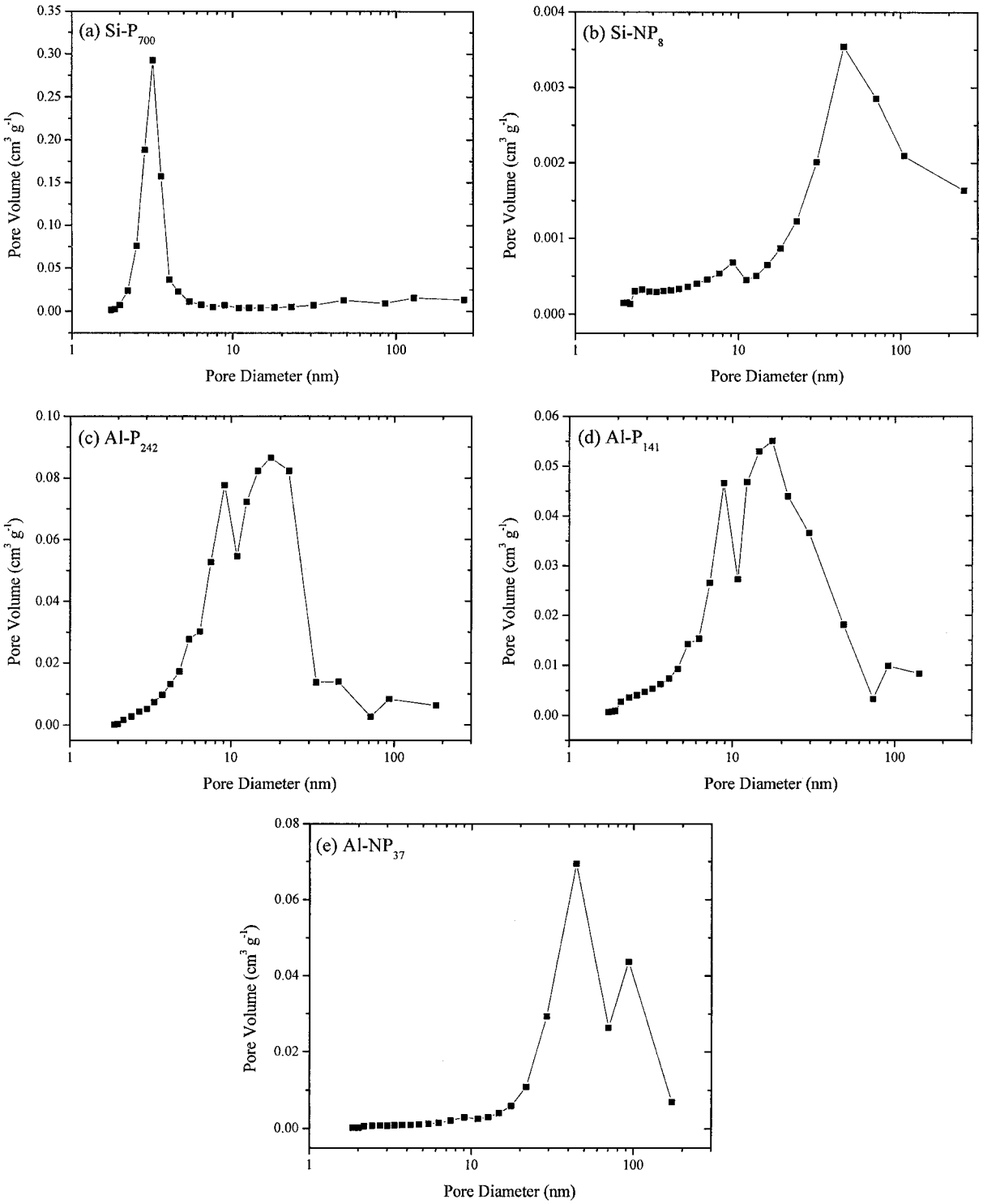

Figure 2. Pore size distribution of adsorbents: (a) Si-P_{700}, (b) Si-NP_8, (c) Al-P_{242}, (d) Al-P_{141}, (e) Al-NP_{37} (calculated from N_2 adsorption branch isotherms using the BJH method [14] and the Halsey layer thickness equation [15]). Note different *y*-axis scales.

mean pore diameter of Si-NP_8 is 14 nm (Table 1) but peak pore volume occurs in pores with diameters of 44 nm (Fig. 2(b)). Both Al-P_{242} and Al-P_{141} have similar pore size distributions with peak pore volumes in 17.5 nm pores (Fig. 2(c) and (d)). However, Al-P_{242} has a lower mean pore diameter and a greater pore volume than Al-P_{141} (Table 1). The large diameters and variability in pore sizes for both Si-NP_8 and Al-NP_{37} (Fig. 2(b) and (e), respectively) is further evidence that these represent textural rather than framework porosity.

Although mesopores are defined as 2–50 nm in diameter, interparticle-pores (20–100 nm) are likely to exist for particles about 100 nm in diameter [23], such as those used in this study. To make an estimate of percent framework porosity, we conservatively define intra-particle pores (mesopores) as those between 2–20 nm in diameter. According to BJH calculations, the great majority of surface area in Si-P_{700}, Al-P_{242} and Al-P_{141} phases is within framework pores (99.7, 96.5, and 92.6%, respectively; Table 1), whereas all of the surface area in Si-NP_8 and Al-NP_{37} phases is found external to mesopores (textural porosity) as indicated by the lack of adsorption/desorption hysteresis. The majority of pore volume in the Si-P_{700}, Al-P_{242} and Al-P_{141} phases is also found within mesopores (2–20 nm; 91.8, 88.3, and 76.0% of total pore volume, respectively). Since our surface charge measurements are conducted in mixed, aqueous particle suspensions, textural porosity effects are expected to be insignificant relative to those derived from framework porosity.

3.2. *XRD and DRIFT Spectroscopy*

Powder XRD analyses for Si-NP_8 and Al-P_{141} yielded broad amorphous humps, indicating that these solids do not exhibit long-range crystalline order. However, mesoporous materials synthesized by the neutral template pathway did yield broad peaks at about 3.4 nm for silica and about 5.1 nm for alumina indicating the presence of somewhat ordered pore walls. Transmission electron microscopy revealed worm-hole-like pores.

DRIFT spectra of the five adsorbents are shown in Fig. 3(a) and (b). The sharp peak in the Si-P_{700} spectrum (Fig. 3(a)) at 3745 cm^{-1} is indicative of terminal ≡SiOH groups [24]. The same peak (3740 cm^{-1}) is greatly diminished in the Si-NP_8 spectrum (Fig. 3(a)). This suggests that on a mass basis Si-P_{700} contains a greater number of terminal hydroxyl groups relative to Si-NP_8, likely as a result of increased SSA. Peaks in the 3675–3540 cm^{-1} wavenumber range can

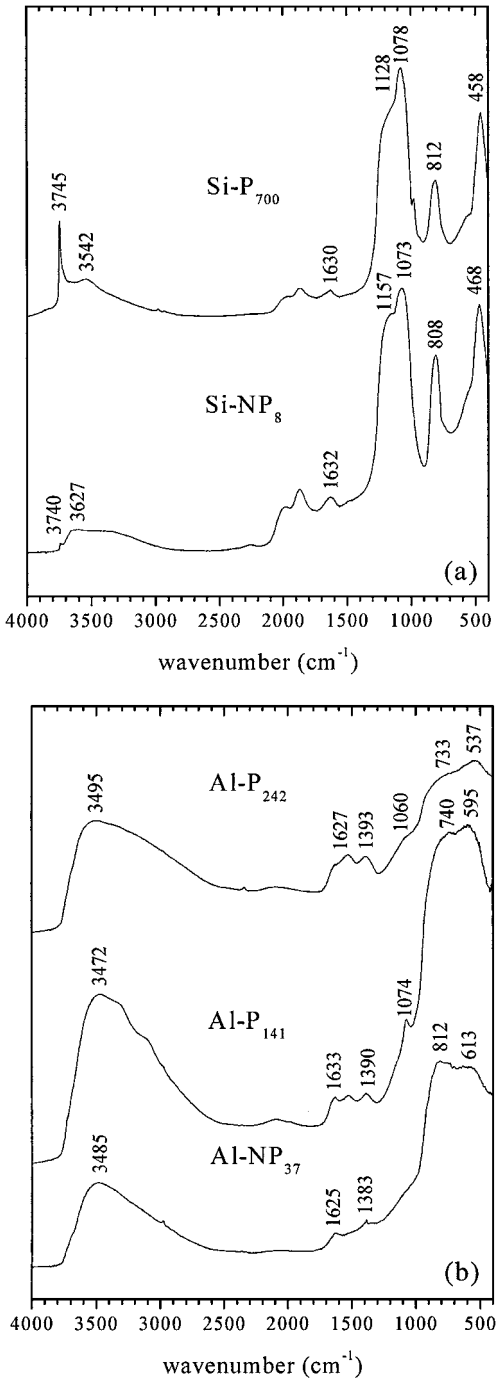

Figure 3. Diffuse reflectance Fourier transform infrared (DRIFT) spectra of: (a) Si-P_{700} and Si-NP_8, (b) Al-P_{242}, Al-P_{141}, Al-NP_{37}.

be attributed to O–H stretching of sorbed water and structural OH, and bending of H–O–H (sorbed water) bonds appear at 1632 and 1630 cm^{-1} in Fig. 3(a) for Si-P_{700} and Si-NP_8, respectively [25, 26]. Peaks in

the lower wavenumber range (1200–400 cm^{-1}) are attributed to Si—O—Si stretching (1200–950 cm^{-1}; [27]), O—H bending of structural OH (950–800 cm^{-1}; [25, 26]), and Si—O—Si bending (550–400 cm^{-1}; [27]).

The DRIFT spectra for the aluminum minerals (Fig. 3(b)) show several interesting trends. The band in the 3495–3470 cm^{-1} frequency range (O—H stretching of sorbed water and structural OH; [25, 26]) increases in intensity relative to peaks in the 815–535 cm^{-1} range (stretching of Al—O in tetrahedral and octahedral coordination; [28, 29]) as framework porosity increases. Bending of H—O—H at ca. 1630 cm^{-1} (Fig. 3(b)) also increases with increasing framework porosity. In addition, there is an emergence of a peak at 1047 cm^{-1} (Al-P_{141}) and a shoulder at 1060 cm^{-1} (Al-P_{242}) that are not present in Al-NP_{37} (Fig. 3(b)). Infrared studies of boehmite have attributed this peak to Al—O—H bending [28, 29], suggesting increased hydroxyl group content in the porous relative to non-porous adsorbents when the two are compared on a mass basis. Lastly, the spectrum for Al-NP_{37} suggests the presence of Al in octahedral (750–500 cm^{-1}; [28, 29]) and tetrahedral coordination (850–750 cm^{-1}; [28, 29]). However, peaks indicative of tetrahedral coordination are absent from Al-P_{141} and Al-P_{242} spectra.

3.3. *Acid-Base Chemistry*

Acid-base titration data for Si-P_{700} and Si-NP_8 show substantial OH^- consumption, relative to the blanks, at pH > 6 (Fig. 4(a)). The buffering of base additions can arise from mineral dissolution and/or surface proton dissociation reactions. Proton dissociation on silanol surface sites starts at circumneutral pH [30] and results in increased negative surface charge [30–32]:

$$\equiv SiOH + OH^- \leftrightarrow \equiv SiO^- + H_2O \qquad (7)$$

Whereas, base consumption due to OH^- promoted dissolution becomes significant at pH > pK_a of silicic acid (pH 9.46; [21]):

$$SiO_2(s) + OH^- \leftrightarrow SiO(OH)_3^- + H_2O \qquad (8)$$

For Al_2O_3 solids, significant H^+ consumption at low values of pH (Fig. 4(b)) may be the result of either proton adsorption [33, 34]:

$$\equiv AlOH + H^+ \leftrightarrow \equiv AlOH_2^+ \qquad (9)$$

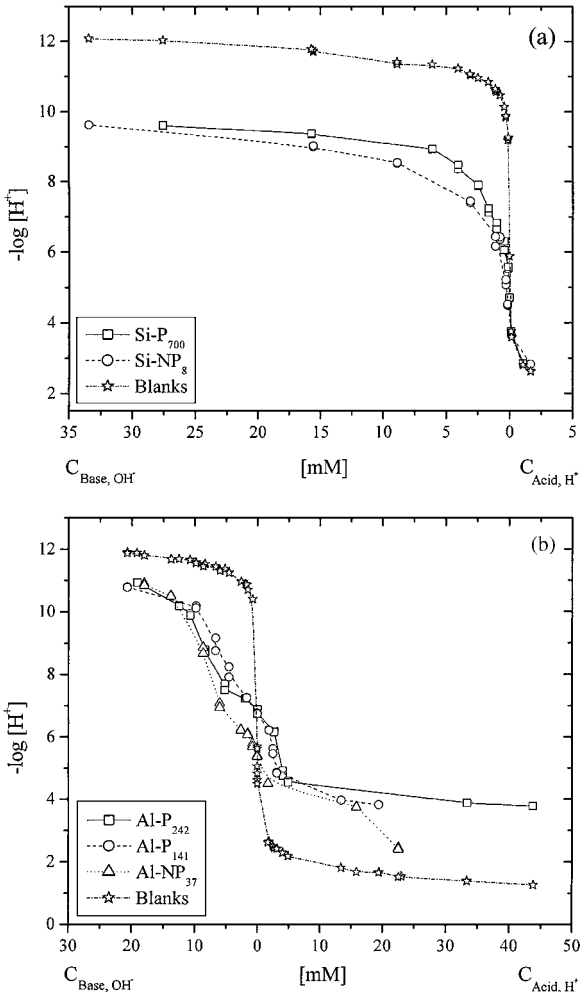

Figure 4. Titration curves showing $-\log [H^+]$ vs. the hydroxide $[OH^-]$ or proton $[H^+]$ concentration added to suspensions of: (a) Si-P_{700} and Si-NP_8, (b) Al-P_{242}, Al-P_{141}, and Al-NP_{37}.

or Al dissolution [35]:

$$0.5\ Al_2O_3(s) + 3H^+ \leftrightarrow Al^{3+} + 1.5\ H_2O \qquad (10)$$

Likewise, at higher pH (>6), base consumption reflects proton dissociation [33, 34]:

$$\equiv AlOH + OH^- \leftrightarrow \equiv AlO^- + H_2O \qquad (11)$$

and/or mineral dissolution [35]:

$$0.5\ Al_2O_3(s) + 1.5\ H_2O + OH^- \leftrightarrow Al(OH)_4^- \qquad (12)$$

Whereas proton adsorption/desorption reactions (Eqs. (7), (9), (11)) give rise to positive/negative

surface charge, mineral dissolution reactions (Eqs. (8), (10), (12)) do not [8]. Further, these two mechanisms of acid-base consumption can not be distinguished on the basis of titration data alone. Distinguishing surface charge development (Eqs. (7), (9), (11)) from mineral dissolution (Eqs. (8), (10), (12)), therefore, requires independent measures of background ion adsorption and framework metal (Al) or metalloid (Si) dissolution.

3.4. Surface Charge Characteristics

Surface excess data for Cl^- (q_-) and Ca^{2+} (q_+) are presented in Fig. 5(a)–(e). The data for Si-P_{700} and Si-NP_8 (Fig. 5(a) and (b), respectively) show negligible adsorption of Cl^- throughout the pH range of the experiments (i.e., $q_- = 0$). In contrast, a sharp increase in Ca^{2+} adsorption occurs at pH > 7, indicating the onset of significant proton dissociation from silanol groups. Negative charge increases exponentially at pH > 8.5. The surface charge behavior of porous Si-P_{700} and non-porous Si-NP_8 is very similar (Fig. 5(a) and (b)), indicating similar densities and reactivities of ≡SiOH groups per unit surface area. At the highest pH studied (9.7) anionic site densities are within the range reported previously for amorphous Si [36–38] and are in excellent agreement with potentiometric titration measurements reported by Karlsson et al. [32]. James and Parks [36] reported surface hydroxyl site densities of 3.5–11 sites nm^{-2} for amorphous silica using several different techniques, whereas Tamura et al. [34] reported values of 5.8 and 9.6 sites nm^{-2} for two amorphous Si minerals using the Grignard reaction method. Zhuravlev [38] employed deuterium exchange to measure surface hydroxyl concentrations for 100 amorphous SiO_2 solids and reported a range of values from 4.0–6.1 sites nm^{-2} for surfaces subjected to the maximum degrees of hydroxylation. As shown in Table 2, the p.z.n.c. values for the Si adsorbents are below the lowest pH employed. This is attributed to the strong acidity of the silica surface, which promotes net cation adsorption to very acidic pH, but no net retention of anions.

Variable surface charge behavior of the Al_2O_3 solids is likewise essentially independent of framework porosity (when normalized to surface area; Fig. 5(c)–(e)). In contrast to SiO_2(s) adsorbents, significant Cl^- adsorption is observed at pH < 7, whereas Ca^{2+} retention increases at pH > 6, and p.z.n.c. values range from 6.5 to 6.9 (Table 2). Evidently, proton consumption and dissociation (Eq. (9) and (11)) predominate below and above the p.z.n.c., respectively. Maximum values of adsorbed Ca^{2+} and Cl^- charge per nm^2 are somewhat lower than most published alumina hydroxyl site densities. For example, Tari et al. [34] and Halter [39] measured 1.75 sites nm^{-2} at pH 6 and 25 sites nm^{-2}, respectively, using potentiometric titration; Tamura et al. [37] reported a value of 19.3 sites nm^{-2} determined using the Grignard reaction method; and Kummert and Stumm [33] measured 8.5 sites nm^{-2} by employing tritium exchange method. However, Kummert and Stumm [33] also measured site density by titration and found that the measured value (1.3 sites nm^{-2}) was significantly less than that determined by tritium exchange (8.5 sites nm^{-2}). Thus, whereas it is possible that the data shown in Fig. 5(c)–(e) underestimate the total density of surface hydroxyl groups, they do provide an accurate measure of active sites for ion exchange [40].

Table 2. Points of zero net charge (p.z.n.c) and points of minimal (p.m.d.) dissolution for the five adsorbents.

Mineral		p.z.n.c.[a]	p.m.d.
Si-P_{700}	$n = 24$	<2.85[b]	<2.85[b]
Si-NP_8	$n = 20$	<2.82[b]	<2.82[b]
Al-P_{242}	$n = 23$	6.47 (±0.05)	6.40[c]
Al-P_{141}	$n = 22$	6.87 (±0.05)	6.40[c]
Al-NP_{37}	$n = 22$	6.66 (±0.06)	6.40[c]

[a]Point of zero net charge (±95% C.I.).
[b]Values of p.z.n.c. or p.m.d. not encountered in the pH range of the experiments. Lowest pH values of experiment are shown.
[c]Values obtained from $[Al]_T$ solubility diagrams (see Fig. 7).

Although the aqueous site density measurements show no discernable differences between the number of surface hydroxyl groups within a mineral type when normalized to surface area, comparisons on a mass basis are very apparent (e.g., 4.0×10^{21} and 5.1×10^{19} sites g^{-1} for Si-P_{700} and Si-NP_8, respectively, at pH 9.5). This result is consistent with differences in DRIFT spectra discussed above, since all IR spectra were collected on the same mass of sample.

As indicated in Eq. (4), $\sigma_H = -\Delta q$ if $\sigma_O \cong 0$. Net proton surface charge densities, σ_H, calculated from Eq. (6) (i.e., acid-base consumption, corrected for mineral dissolution) are compared with $-\Delta q$ (Eqs. (3), (5)) in Fig. 6(a)–(e). These two independent measurements of variable surface charge agree reasonably well in the intermediate pH range although some discrepancies exist at high and low pH. Discrepancies increase with increasing mineral dissolution, as indicated by

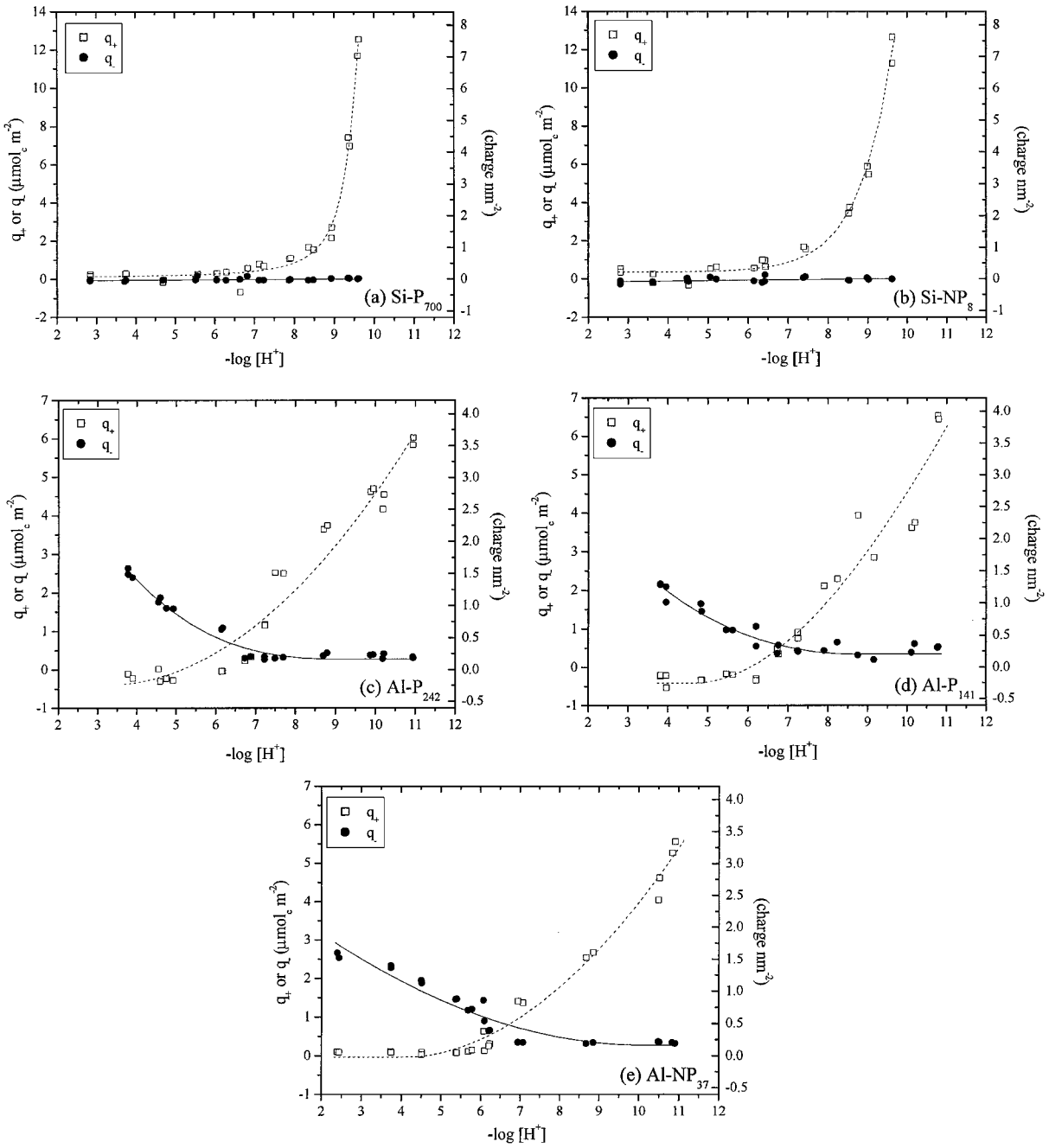

Figure 5. Adsorbed ion charge density of q_+ and q_- as a function of $-\log [H^+]$: (a) Si-P_{700}, (b) Si-NP_8, (c) Al-P_{242}, (d) Al-P_{141}, (e) Al-NP_{37}.

comparing dissolution data (Fig. 7) with Fig. 6. Relative to net adsorbed ion charge (Δq) measurements, proton titration data (σ_H) under-predict the magnitude of negative surface charge at high pH for all samples and over-predict positive charge at low pH for mesoporous Al_2O_3 samples (Fig. 6). This is despite the fact that σ_H was corrected for Al or Si dissolution. In addition, because of the log-linear relation between $[H^+]$ and emf, small emf measurement errors at high and low pH may result in large errors in

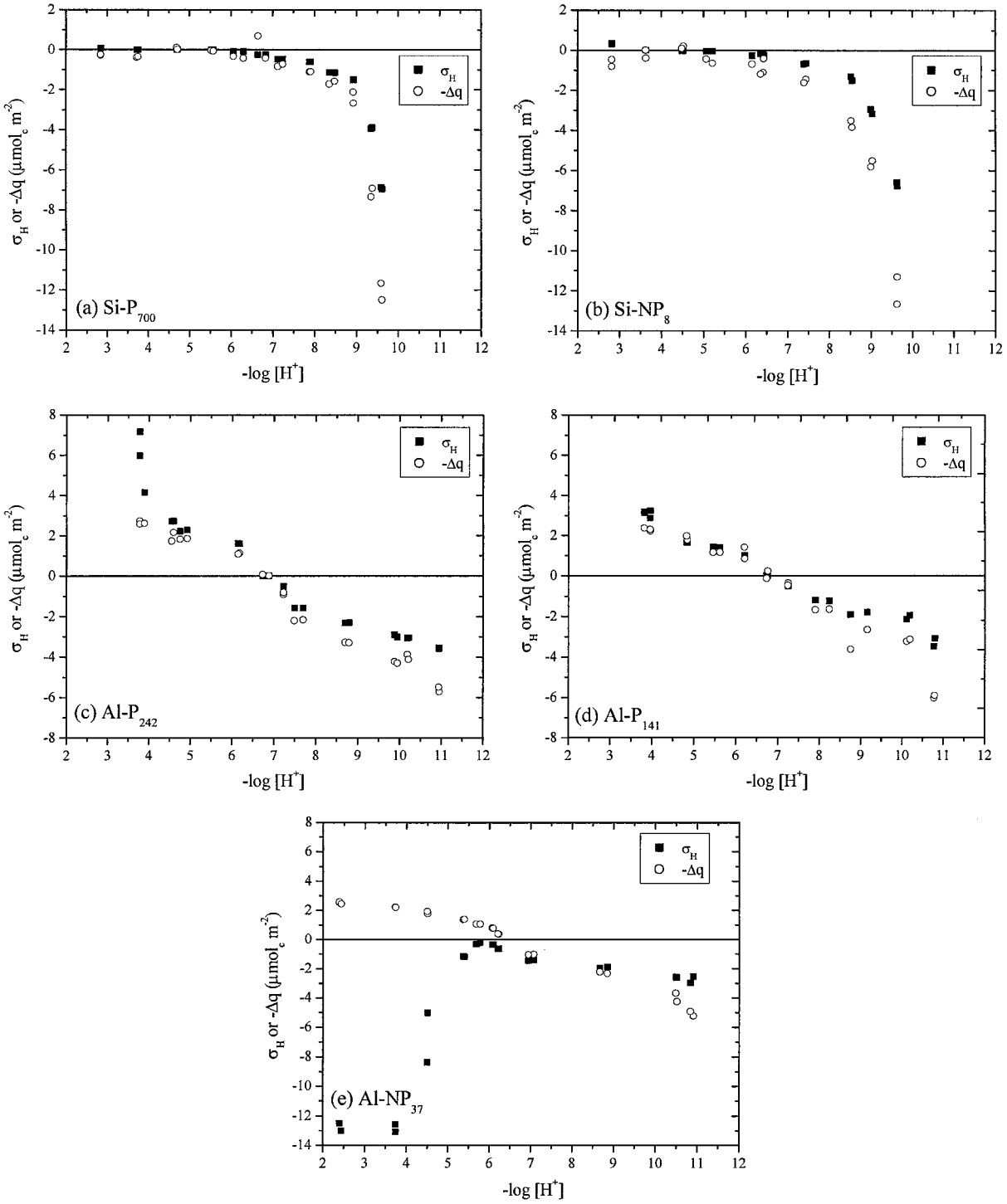

Figure 6. Apparent proton surface charge density (σ_H), corrected for Al or Si dissolution, and negative net adsorbed ion charge density ($-\Delta q$) as a function of $-\log [H^+]$: (a) Si-P_{700}, (b) Si-NP_8, (c) Al-P_{242}, (d) Al-P_{141}, (e) Al-NP_{37}.

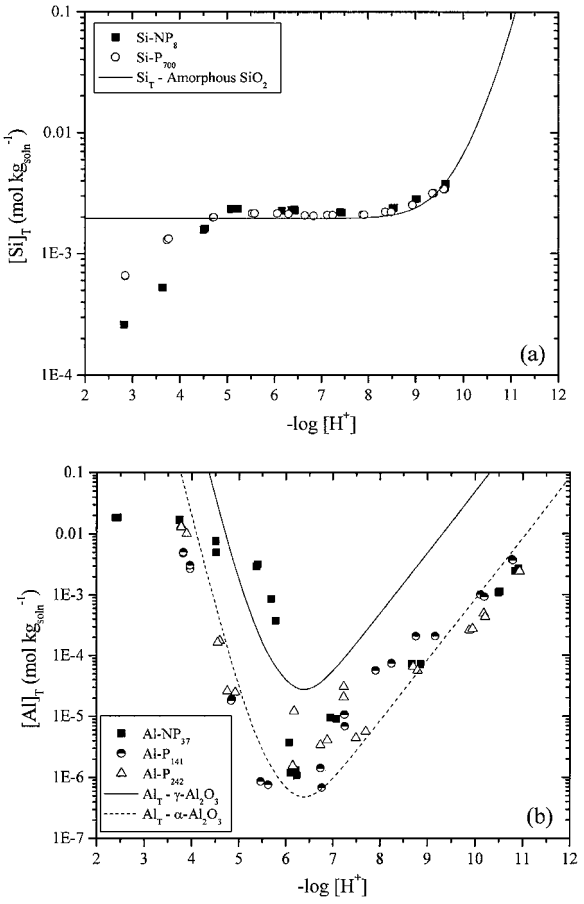

Figure 7. Dissolution of (a) Si-P_{700} and Si-NP_8 with respect to amorphous SiO_2 (log $K_{sp} = -2.71$; [20]) and (b) Al-P_{242}, Al-P_{141}, Al-NP_{37} with respect to γ-Al_2O_3 (log $K_{sp} = 11.49$; [32]) and α-Al_2O_3 (log $K_{sp} = 9.73$; [32]). Hydrolysis constants for Al and Si were obtained from Nordstrom and May [19] and Stumm and Morgan [20], respectively.

σ_H as calculated from Eq. (6). The data are in agreement where $\sigma_H = -\Delta q = 0$, indicating that for these variable-charge minerals p.z.n.c. = p.z.n.p.c.

The drastic Al over-correction for σ_H in Fig. 6(e) is attributed to dispersion of positive-charged colloids at low pH. Transmission electron micrographs of Al-NP_{37} show spherical primary particles of diameter ca. 37 nm, which may have passed through the 0.2 μm nominal pore size filter prior to ICP analysis and calculation of σ_H by Eq. (6). The data in Fig. 7(b) suggest Al concentrations for several samples exceed values expected to occur in equilibrium with γ-Al_2O_3 and α-Al_2O_3. This apparent over-saturation is attributed to microcolloidal material in filtrates. As a result, we suggest that adsorbed ion charge measurements more accurately reflect the actual surface charge characteristics of the minerals investigated.

4. Conclusions

The effects of framework porosity on surface charge were investigated for SiO_2 and Al_2O_3 solids comprising framework pore volumes ranging from 0.008 to 0.85 $cm^3\ g^{-1}$ (SiO_2) and 0.06 to 0.50 $cm^3\ g^{-1}$ (Al_2O_3). Despite large differences in specific surface areas and porosities, surface charge behavior was very consistent for a given adsorbent chemical composition, when data were normalized to surface area. These results suggest that reactive (i.e., protonating and dissociating) silanol or aluminol groups populate the surface of these adsorbents to an extent that is unaffected by mesoporosity. Uptake of ionic solutes from aqueous solution is, therefore, expected to scale linearly with the increase in specific surface area for a fixed mass of porous material. This work also underlines the potential shortcomings associated with assessment of surface charge solely on the basis of proton titration.

Acknowledgments

The authors thank Mary Kay Amistadi for assistance and Stephen Stout for aiding in mineral preparation. Financial support was provided by the Penn State Biogeochemical Research Initiative for Education (BRIE) sponsored by NSF (IGERT) Grant DGE-9972759, the Penn State Materials Research Science and Engineering Center (MRSEC) sponsored by NSF Grant DMR-0080019, and the Penn State Materials Research Institute (MRI).

References

1. A.C. Walcarius, C. Despas, and J. Bessière, Microporous and Mesoporous Mater. **23**, 309 (1998).
2. H.H.P. Yiu, P.A. Wright, and N.P. Botting, Microporous and Mesoporous Mater. **44/45**, 763 (2001).
3. J.C. van der Waal and H. van Bekkum, J. Porous Mater. **5**, 289 (1998).
4. N. Srinivas, V.R. Rani, S.J. Kulkarni, and K.V. Raghavan, J. Mol. Catal. A: Chem. **17**, 221 (2002).
5. S. Komarneni, R. Pidugu, and V. Menon, J. Porous Mater. **3**, 99 (1996).
6. H. Zhao, K.L. Nagy, J.S. Waples, and G.F. Vance, Environ. Sci. Technol. **34**, 4822 (2000).

7. K.W. Goyne, J. Chorover, S.L. Brantley, and S. Komarneni, in Eleventh Annual V.M. Goldschmidt Conference 2001, abstract no. 3413 (LPI Contribution No. 1088, Lunar and Planetary Institute, Houston, available on CD-ROM).
8. W. Stumm, *Chemistry of the Solid-Water Interface* (John Wiley and Sons, New York, 1992).
9. G. Sposito, in *Environmental Particles*, Vol. 1, edited by J. Buffle and H.P. van Leeuwen (Lewis Publishers, Boca Raton, 1992), p. 291.
10. G. Sposito, *The Chemistry of Soils* (Oxford University Press, New York, 1989).
11. G. Sposito, Environ. Sci. Technol. **32**, 2815 (1998).
12. P.T. Tanev and T.J. Pinnavaia, Chem. Mater. **8**, 2068 (1996).
13. W. Zhang, T.R. Pauly, and T.J. Pinnavaia, Chem. Mater. **9**, 2491 (1997).
14. K.S.W. Sing, D.H. Everett, R.A.W. Haul, L. Moscou, R.A. Pierotti, J. Rouquerol, and T. Siemieniewska, Pure Appl. Chem. **57**, 603 (1985).
15. E.P. Barrett, L.J. Joyner, and P.P. Helenda, J. Am. Chem. Soc. **73**, 373 (1951).
16. G.D. Halsey, J. Chem. Phys. **16**, 931 (1948).
17. J. Chorover and G. Sposito, Geochim. Cosmochim. Acta **59**, 875 (1995).
18. S. Sjoberg, Y. Hagglund, A. Nordin, and N. Ingri, Mar. Chem. **13**, 35 (1983).
19. M.G. Keizer and W.H. van Riemsdijk, *ECOSAT, a Computer Program for the Calculation of Speciation and Transport in Soil-Water Systems: Version 4.7* (Wageningen University, The Netherlands, 1999).
20. D.K. Nordstrom and H.M. May, in *The Environmental Chemistry of Aluminum*, 2nd edn., edited by G. Sposito (Lewis Publishers, Boca Raton, 1996), p. 39.
21. W. Stumm and J.J. Morgan, *Aquatic Chemistry*, 3rd edn. (John Wiley and Sons, New York, 1996).
22. S. Brunauer, *The Adsorption of Gases and Vapors, Vol. I: Physical Adsorption* (Princeton University Press, Princeton NJ, 1943).
23. J.H. Conway, N.J.A. Sloane, *Sphere Packings, Lattices, and Groups*, 2nd edn. (Springer-Verlag, New York, 1993).
24. C.M. Koretsky, D.A. Sverjensky, J.W. Salisbury, and D.M. D'Aria, Geochim. Cosmochim. Acta **61**, 2193 (1997).
25. J.L. White and C.B. Roth, in *Methods of Soil Analysis*, Part 1, 2nd edn., edited by A. Klute (ASA, Madison, 1986), p. 291.
26. C.T. Johnston and Y.O. Aochi, in *Methods of Soil Analysis*, Part 3, edited by D.L. Sparks (SSSA, Madison, 1996), p. 269.
27. H.H.W. Moenke, in *The Infrared Spectra of Minerals*, edited by V.C. Farmer (Mineralogical Society, London, 1974), p. 365.
28. G.K. Priya, P. Padmaja, K.G.K. Warrier, A.D. Damodaran, and G. Aruldhas, J. Mater. Sci. Lett. **16**, 1584 (1997).
29. Ph. Colomban, J. Mat. Sci. **24**, 3002 (1989).
30. R.K. Iler, *The Chemistry of Silica* (John Wiley and Sons, New York, 1979).
31. P.V. Brady and J.V. Walther, Geochim. Cosmochim. Acta **53**, 2823 (1989).
32. M. Karlsson, C. Craven, P.M. Dove, and W.H. Casey, Aq. Geochem. **7**, 13 (2001).
33. R. Kummert and W. Stumm, J. Colloid Interface Sci. **75**, 373 (1980).
34. G. Tarì, S.M. Olhero, and J.M.F. Ferreira, J. Colloid Interface Sci. **231**, 221 (2000).
35. W.L. Lindsay, *Chemical Equilibria in Soils* (Wiley, New York, 1979).
36. R.O. James and G.A. Parks, in *Surface and Colloid Science*, Vol. 12, edited by E. Matijević (Plenum Press, New York, 1982), p. 119.
37. H. Tamura, A. Tanaka, K. Mita, and R. Furuichi, J. Colloid Interface Sci. **209**, 225 (1999).
38. L.T. Zhuravlev, Colloids and Surfaces **173**, 1 (2000).
39. W.E. Halter, Geochim. Cosmochim. Acta **63**, 3077 (1999).
40. S. Goldberg, J.A. Davis, and J.D. Hem, in *The Environmental Chemistry of Aluminum*, 2nd edn., edited by G. Sposito (Lewis Publishers, Boca Raton, 1996), p. 271.